IEEE Robotics and Automation Letters (RAL) paper presented at the
2020 IEEE/RSJ International Conference on Intelligent Robots and Systems (IROS)
October 25-29, 2020, Las Vegas, NV, USA (Virtual)

Lightweight High Voltage Generator for Untethered Electroadhesive Perching of Micro Air Vehicles

Sanghyeon Park
Dept. Electrical Engineering
Stanford University
Stanford, California 94305
Email: spark15@stanford.edu

Daniel S. Drew
Dept. Mechanical Engineering
Stanford University
Stanford, California 94305
Email: dsdrew@stanford.edu

Sean Follmer
Dept. Mechanical Engineering
Stanford University
Stanford, California 94305
Email: sfollmer@stanford.edu

Juan Rivas-Davila
Dept. Electrical Engineering
Stanford University
Stanford, California 94305
Email: jmrivas@stanford.edu

***Abstract*—The limited in-flight battery lifetime of centimeter-scale flying robots is a major barrier to their deployment, especially in applications which take advantage of their ability to reach high vantage points. Perching, where flyers remain fixed in space without use of flight actuators by attachment to a surface, is a potential mechanism to overcome this barrier. Electroadhesion, a phenomenon where an electrostatic force normal to a surface is generated by induced charge, has been shown to be an increasingly viable perching mechanism as robot size decreases due to the increased surface-area-to-volume ratio. Typically electroadhesion requires high (> 1 kV) voltages to generate useful forces, leading to relatively large power supplies that cannot be carried on-board a micro air vehicle. In this paper, we motivate the need for application-specific power electronics solutions for electroadhesive perching, develop a useful figure of merit (the "specific voltage") for comparing and guiding efforts, and walk through the design methodology of a system implementation. We conclude by showing that this high voltage power supply enables, for the first time in the literature, tetherless electroadhesive perching of a commercial micro quadrotor.**

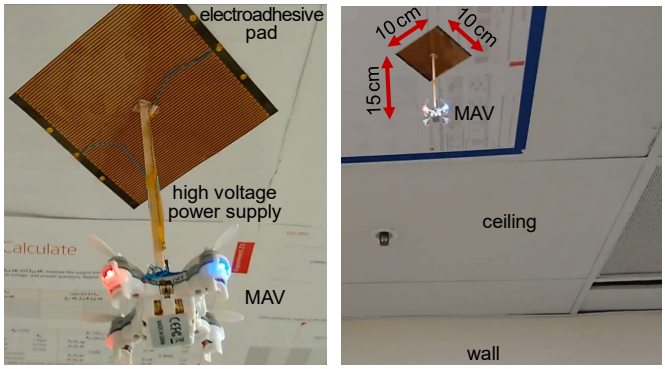

(a) (b)

Fig. 1. Flight and electroadhesive perching of a commercially available micro-quadrotor presented in this paper, which can extend mission lifetime from minutes to hours. (a) Close-up view of the quadrotor. (b) Wide view.

I. Introduction

Micro air vehicles (MAVs), generally defined as unmanned aerial vehicles (UAVs) with characteristic lengths less than 15 cm [1], are emerging platforms with potential application spaces ranging between search and rescue operations, natural disaster recovery efforts, precision agriculture, and urban traffic monitoring [2]–[4]. Real-world deployment of MAVs is challenged by their extremely limited single-charge flight time: due to a combination of effects of miniaturization including decreased motor and aerodynamic efficiency and an increase in the proportion of payload budget required for control electronics, the flight time of a MAV is typically measured in minutes [5]. Implementing MAV behavioral patterns which can minimize energy consumption during task performance is therefore an attractive method to extend mission lifetime without relying on significant advances in propulsion or energy storage.

The most significant fraction of a MAV power budget is allocated to flight actuators; in the case of a quadrotor, the four DC motors driving the propellers. Implementing multimodal locomotion strategies – switching from flying to "walking" – is one proposed method for conserving energy [6]. Many tasks, however, rely on the high vantage point afforded by a flying robot. At the same time, many of these (typically vision-based) tasks do not require frequent position updates; in fact, many take advantage of the ability of a quadrotor to hover in place and suffer from the challenge small robots face in remaining fixed during adverse atmospheric conditions. Perching, a natural behavior exhibited by many flying animals, is a potential method for future robots to retain the vantage point benefits of flight while drastically reducing actuator energy usage and increasing stability [7], [8].

Among other methods used for perching (e.g., avian-inspired grasping [9]), electrostatic adhesion, also known as electroadhesion, is particularly promising for small-sized vehicles due to its simple mechanical and electrical mechanism. Electroadhesive perching has been previously demonstrated for an insect-scale flyer on a variety of attachment surfaces [10] while powered by an external supply; this work was motivated by the fact that electroadhesion is a surface area dominated force, which means it benefits from the increasing surface-area-to-volume ratio that results from

This material is based upon work supported by the National Science Foundation under Grant No. 1808489 and by the Intelligence Community Postdoctoral Research Fellowship Program, administered by Oak Ridge Institute for Science and Education through an interagency agreement between the U.S. DoE and the ODNI.

decreasing robot size [11]. Furthermore, electroadhesion is switchable, consumes very low power, and has been shown to be effective for a wide range of surface materials, surface roughness, and moisture levels [12], [13].

The attachment force for an electroadhesive pad scales with the square of the electric field (and therefore bias voltage), and pads with forces relevant to perching of MAVs ($\approx$ 10 to 100 gf) typically require voltages on the order of several kilovolts for initial substrate attachment. This high voltage requirement often leads to unwieldy conversion electronics that are no longer suitable for flying, especially with the relatively small payload capacity of a MAV. This challenge means that, while at-scale electroadhesion with normal adhesive forces well in excess of MAV weights has been shown, there has been no demonstration to-date of electroadhesive perching of a MAV without an external power supply. In order to support this functionality in future autonomous platforms, a new type of power supply is required.

In this paper, we first use application-specific design constraints in order to establish a new figure of merit which can be used for assessing and guiding development of high voltage generators appropriate for functions like electroadhesion and other electrostatic-force based effects (e.g., dielectric elastomer actuation). This figure of merit is used as the guiding principle behind the design of a 4.3 kV dc voltage generator, based on a resonant topology previously described in [14], that operates on a single-cell lithium polymer battery input and masses 951 mg. Relevant design tradeoffs and the overall design methodology are detailed for researchers to replicate or modify this process in order to suit individual operation points. We place the supply shown in this work, as well as a broad set of commercial and research grade high voltage supplies, in a design landscape relevant to tetherless electroadhesive perching and, more generally, to high voltage generation on-board payload constrained robots. Lastly, we demonstrate electroadhesive perching of a commercially available micro-quadrotor while streaming video from its on-board camera (shown in Fig. 1). To our knowledge, this is the first time that untethered electroadhesive perching of a MAV has been demonstrated; it proves that with proper design of the power system, it is possible to add this perching capability to existing platforms even using fully commercially-available circuit components.

II. Evaluating Power Supplies for Electroadhesive Perching

Due to their unique operating point (i.e., high voltage ratio and low power) and unique design constraints (i.e., system volume and mass within the capacity of a small flying robot), power supplies for electroadhesive perching should be evaluated differently than power supplies for other applications.

A. Proposed figure of merit

Widely used figures of merit for power supplies such as power density, specific power, or power conversion efficiency are not directly useful for evaluating their capacity for electroadhesive perching. Here, we develop a relevant figure of merit based on two task-specific properties: Firstly, the electroadhesive pad consumes very little power during operation (typically $<$ 1 mW), because as an electrostatic effect the only current flowing through the pad is due to leakage. As a result, the design of the power supply is rarely limited by its thermal (i.e, power handling) performance. The voltage required for electroadhesive perching, however, is usually in the range of several kilovolts, meaning a high voltage gain is necessary. As a consequence of this low power consumption and high voltage requirement, the mass of a power supply for electroadhesion is largely determined by its output voltage; the voltage gain ratio, as well as the increased component-to-component spacing and insulation thickness required to prevent dielectric breakdown, are the primary drivers. Secondly, the mass of the supply must be low enough that it can be carried by the robot; for perching to be a useful functional addition, it must not require excessive payload capacity that could have been spent on, for example, additional energy storage. In order to compare this work with others in the context of electroadhesive perching, we propose a new figure of merit (FOM) as:

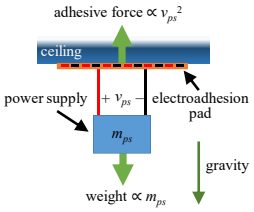

Fig. 2. Depiction of a power supply with a mass m_{ps} and an output voltage v_{ps}, hanging from the substrate by an electroadhesive force. The proposed figure of merit represents the ratio of the adhesive force to the weight.

$$\text{FOM} = v_{ps}^2/m_{ps} \tag{1}$$

where m_{ps} denotes the power supply's mass and v_{ps} its output voltage that drives the adhesive pad. This proposed figure of merit will be referred to as the *specific voltage* in subsequent sections.

As depicted in Fig. 2, the specific voltage indirectly relates the achievable adhesive force to the weight of the power supply. The FOM is defined this way because the adhesive force is proportional to v_{ps}^2 [12], [15], [16] and, assuming the pad and the supporting structure are of negligible mass compared to the power supply, the gravitational force downward is proportional to m_{ps}. This assumption is justified by noting that electroadhesive pads are fabricated using thin-film technology; for example, polyimide and Paralyene film layers with sub-micron thickness metal in between yields $\approx$ 3 mg/cm^2 high-performance pads in [10]. The definition is similar to a thrust-to-weight ratio for evaluating propulsive actuators in that the "upward" force is compared with respect to the "downward" force.

We can use this specific voltage FOM to compare our work with various off-the-shelf and research-grade miniature power supplies (see Appendix for full list). As shown in

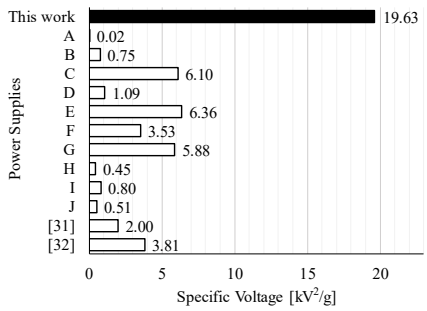

Fig. 3. Comparison of our work to commercially available miniature power supplies and research-grade power supplies by the proposed FOM. See Appendix for the full list of power supplies. (full list omitted to meet the IROS page limit; see RA-L version of this paper)

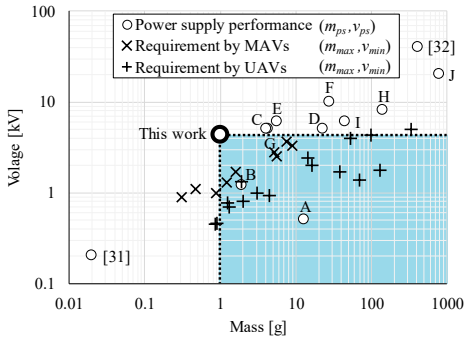

Fig. 4. Mass and output voltage of high voltage power supplies. ○ marks indicate performances reported in this work and previous publications. × marks and + marks indicate performances required by published MAV and UAV designs, respectively. See Appendix for the full list.

Fig. 3, the specific voltage of our power supply is several times higher than any other commercially available converter. This has important implications on the capability for adding electroadhesion to existent MAV platforms, which will be highlighted in the following section.

B. Impact of the presented power supply

In order to evaluate the potential impact of our proposed power supply, as well as to motivate development of supplies with similar figures-of-merit, we develop design criterion for voltage supplies suitable for electrostatic MAV perching. Firstly, the mass of the power supply should be within the payload capacity of the robot. Due to the rising proportional mass allocation required for control autonomy and actuators at the MAV scale and below [17], the payload capacity dedicated to perching must be relatively small. Secondly, the power supply must generate a voltage that is high enough to provide a sufficient attaching force; this specific requirement scales with robot characteristic length (due to the change in surface area and mass). Lastly, the power supply should be able to run directly from the existing battery; incorporation of an additional energy storage source (with associated overhead) to enable perching is an inefficient use of already highly-constrained resources. Existing commercial high voltage supplies typically require a supply voltage exceeding what a single cell lithium polymer battery can provide.

Fig. 4 illustrates with ○-marks the mass and the output voltage of various high voltage power supplies. Plotted together with ×-marks and +-marks are maximum-acceptable masses and minimum-required voltages of the power supply as derived from published MAV ($\leq$ 15 cm) and UAV ($>$ 15 cm) designs, respectively. Our work (large ○ mark) is notably located at the top-left side of the plot, which is directly related to the high FOM as demonstrated in the previous section. The area shaded in blue, which includes the majority of MAVs, indicates the design space for which untethered electroadhesive perching becomes possible using the presented power supply.

The maximum-acceptable supply mass, m_{ps}, is derived by assuming that one-tenth of the vehicle's mass is the acceptable upper bound of the payload added by the power supply. This condition is expressed in an equation as follows:

$$m_{max} = \left(\frac{1}{10}\right) m_{mav} \geq m_{ps} \tag{2}$$

where m_{max} denotes the maximum-acceptable mass of the power supply, m_{mav} the mass of the MAV, and m_{ps} the mass of the power supply.

Second, we assume that the surface area of an electroadhesive pad A_{pad} is equal to the square of the vehicle's tip-to-tip length l_{mav}, i.e.,

$$A_{pad} = l_{mav}^2 \tag{3}$$

This area can be considered the upper bound of a realistic pad size for a MAV; it is likely an overestimate that becomes increasingly inaccurate with increasing vehicle size due to aerodynamic effects and surface contact uniformity challenges.

For deriving the minimum output voltage of the power supply the worst-case normal adhesion pressure needs to be assumed. Previous publications report many different adhesion pressures for the worst-case scenario, including 15.6 Pa at 1 kV potential for unfinished plywood [10], 15 Pa at 3 kV for woven cotton [12], and 2 kPa at 4 kV potential for damp concrete [18]. Here, we assume that the condition in [10] holds. For an arbitrary voltage v_{ps} applied to the pad, the adhesive force F_N is then given by:

$$F_N = (15.6 \text{ Pa}) A_{pad} \left(\frac{v_{ps}}{1 \text{ kV}}\right)^2. \tag{4}$$

Noting the strong effect of surface material and contact conditions on adhesion, the estimated adhesive force should be several times larger than the vehicle weight in order to guarantee reliable operation. There is no definite consensus on the optimal 'safety factor', i.e., the worst-case force to weight ratio. Existing publications on robots walking on or perching to a ceiling use a safety factor ranging from 2.7 to 4.1 [10], [15], [18]–[20]. In this analysis, we use a safety factor of 4 following the design process from [15], [18], [20]. Then, the condition can be written as:

$$F_N \geq 4 m_{mav} (9.8 \text{ m/s}^2). \tag{5}$$

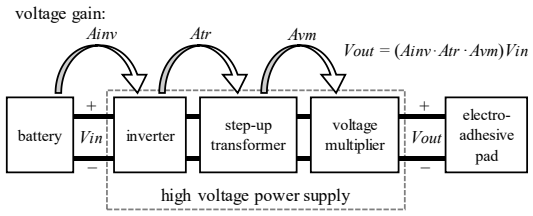

Fig. 5. Typical structure of a high voltage power supply for electroadhesion.

Plugging in (3) and (4) to (5) and solving for the minimum-required voltage from the power supply v_{min}, we obtain:

$$v_{min} = (1\text{ kV})\sqrt{\frac{4m_{mav}(9.8\text{ m/s}^2)}{l_{mav}^2(15.6\text{ Pa})}} \leq v_{ps}. \qquad (6)$$

Calculating (m_{max}, v_{min}) for each vehicle in the survey (See Appendix for the full list) yields the result depicted in Fig. 4. Note that neither Fig. 4 nor the proposed FOM captures the allowable level and variation of the input voltage, which is an important aspect of the circuit performance and overall system analysis. Providing a regulated voltage input at or above the existing battery level would require additional payload mass.

III. High Voltage Power Supply Design Process

This section is intended as a resource to aid in replicability and modification of the presented high voltage generator. Importantly, the presented supply is achieved using entirely off-the-shelf components and a commercially-fabricated flexible printed circuit board (PCB); both the bill of materials and the board layout files are available at `https://code.stanford.edu/super-lab-public/2020_spark_lightweight_hv_gen`.

A. Component- and topology-based performance trade-offs

Fig. 5 shows the structure of a high voltage power supply driving an electroadhesive pad. The power supply consists of an inverter, a step-up transformer, and a voltage multiplier. Assuming a single-cell lithium polymer battery on the vehicle as the power source, the input dc voltage V_{in} for the inverter is about 3.7 V. The inverter converts this dc voltage to an ac voltage with a gain of A_{inv}. The transformer amplifies the ac voltage by a factor of A_{tr}. The voltage multiplier then multiplies the ac voltage by a factor of A_{vm} and rectifies it to a dc potential V_{out} that is $(A_{inv} \cdot A_{tr} \cdot A_{vm})$ times larger than V_{in}.

Table I summarizes the trade-off relationship between various topologies for the inverter, transformer, and multiplier. The relationship is presented qualitatively rather than quantitatively because, for discrete circuits, the mass and volume are heavily affected by availability of parts in the market and thus are not suitable for parametric modeling. In general, a topology with a higher voltage gain is larger in size and mass than one with a lower gain. To maintain an overall target gain, the choice of one topology with a lower gain must be compensated by another topology with a higher gain in a different part of the circuit. Designing

TABLE I
Trade-off relationship between various topologies for the inverter, the transformer, and the voltage multiplier.

size & weight	**voltage gain**	**inverter**	**step-up transformer**	**voltage multiplier**
small & light	low	half bridge	few turns	few high-voltage stages
		↓ full bridge ↓ class-E ↓		
big & heavy	high	push-pull class-E	many turns	many low-voltage stages

a lightweight high voltage generator (i.e., one with a high specific voltage) can be seen as an optimization problem to find the best combination of topologies that achieves the desired outcome.

A concrete example of this tradeoff can be shown for the selection of an inverter: a push-pull class-E has a dc-to-ac voltage gain of 6, which is the highest among switch-mode inverter topologies (50% duty cycle is assumed). From there, by decreasing gain (and therefore also decreasing mass), is the single-ended class-E inverter's gain of 3, a full-bridge inverter's gain of 2, and a half-bridge's gain of 1. In this case, the main factor that shapes this trade-off between voltage gain and mass is the number of inductors in each topology. Two choke inductors are necessary to build a push-pull class-E inverter while one is sufficient for a single-ended class-E, and none for a half-bridge or a full-bridge. Moreover, half-bridge and full-bridge inverters do not require any high-value external passive components, thus can be implemented as simply as one or two integrated circuit (IC) chips.

For the transformer, the designer has to consider not only the number of windings but also the mass of the magnetic core. The magnetic core's mass cannot be reduced indefinitely because it needs to store a certain amount of energy during the charging-discharging cycle of the voltage multiplier. Ideally, the peak energy stored in the core is determined solely by the power consumption of the voltage multiplier, which is nearly zero when it comes to electroadhesion. However, any real voltage multiplier has an input capacitance that loads the transformer with reactive power. This capacitance increases with the number of capacitors and diodes, meaning more stages in the multiplier necessitates a heavier magnetic core. Additionally, this charging-discharging current is proportional to the switching frequency and the voltage amplitude from the inverter, which means the choice of a higher-gain inverter topology may increase the necessary mass of the core.

For the voltage multiplier, a design consisting of many low-voltage stages has an advantage of low voltage stress on capacitors and diodes (a *stage* refers to a rectifier circuit that consists of two capacitors and two diodes, which serves as a basic building block for the voltage multiplier). Because lower-voltage components are more likely to be available in a smaller package, the multiplier design can be small and light

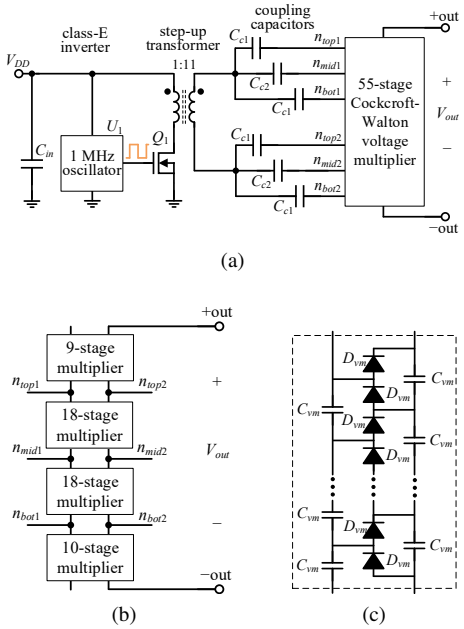

Fig. 6. Schematic of the implemented high voltage power supply. (a) Overall structure. (b) 55-stage voltage multiplier with taps in the middle. (c) Detailed structure of the Cockcroft-Walton multiplier.

TABLE II
PARTS LIST FOR THE HIGH VOLTAGE POWER SUPPLY. PART NAMES ARE IN REFERENCE TO FIG. 6.

Name	Description
U_1	SiT8924B, 1 MHz oscillator, SiTIME
C_{in}	4.7 µF, X5R, 10 V, 0402 package
Q_1	SSM3K56CT, 20 V 800 mA NMOS, Toshiba
transformer	UA7868-AE, 1:11 coupled inductor, Coilcraft
C_{c1}	1.5 nF, X7R, 3 kV, 1808 package
C_{c2}	1.5 nF, X7R, 630 V, 0603 package
C_{vm}	10 nF, 50 V, X5R, 0201 package
D_{vm}	DLLFSD01LP3-7, 80 V 100 mA, Diodes Inc.

despite higher component counts compared to an implementation with few high-voltage stages. More multiplier stages mean a higher ac-to-dc voltage gain, which allow lighter and smaller topologies for the inverter and transformer (subject to the constraints on transformer design noted above).

B. Circuit design methodology

In this section, all part names and circuit structures are in reference to Fig. 6 and Table II.

The design of the power supply begins with selection of the inverter topology. We choose a class-E inverter with integrated magnetic components [21]–[23], which resembles a flyback converter in structure. This topology uses the magnetizing inductance of the step-up transformer for the resonant operation, thus can be implemented without a separate choke inductor unlike a conventional class-E. This absence of an inductor is a huge benefit in terms of saving mass. The inverter provides roughly a gain of 3, converting 3.7 V dc to a 11 V ac peak-to-peak.

The resonant operation of the class-E inverter demands that the transistor Q_1 withstand roughly 3 times the input dc voltage. Since a 3.7 V input from the battery is assumed, Q_1 should be rated at least 11 V. Considering safety margin, we choose a 20 V rated MOSFET.

Next, we find transformers with the highest gain and the lowest mass among their product series. Then we judge whether a higher gain is worth the additional mass that comes with it while considering the then-allowable reduction in mass of the inverter and/or the multiplier. Following this process, we choose a part with a 1-to-11 step-up ratio and 52 mg mass. This transformer boosts the 11 V ac from the inverter to a 120 V ac peak-to-peak.

The transformer ac voltage is delivered to the multiplier via coupling capacitors C_{c1} and C_{c2} with 1.5 nF value. Using 1.5 nF is the result of balancing a trade-off between the capacitor's mass and the multiplier's output impedance. For C_{c1}, we choose the smallest available capacitor among the parts rated at least 2.1 kV, which is the nominal voltage stress on the capacitor (1.4 kV) plus a 50% safety margin.

Finally, we design the multiplier. The expected voltage stress on the diodes and capacitors of the multiplier is roughly the same as the peak-to-peak amplitude of the transformer output. Among parts that can withstand 120 V, we select ones in the smallest package to minimize the mass of components and the mass of a circuit board that is needed for assembly.

We proceed to determine the number of stages in the voltage multiplier. A multiplier consisting of n stages has an ac-to-dc voltage gain of n under no-load condition. In this design, we use 55 stages so that the 120 V ac from the transformer is multiplied by 55, resulting in about 6.6 kV dc output. In reality, the output voltage is lower than that because of the loading effect [24]–[26]. It should be noted that the number of stages cannot be increased without limit, otherwise excessive voltage stress will be placed on the coupling capacitors which bridge between the transformer and the multiplier.

Then, we check the behavior of the voltage multiplier to find the optimal driving condition. Specifically, we measure the output voltage of the multiplier while varying the frequency and amplitude of the input voltage. In general, the higher the switching frequency of the voltage multiplier the better because of the smaller output impedance. However, the frequency cannot be increased indefinitely due to the diodes' reverse recovery as well as the reactive loading on the transformer by the multiplier's input capacitance. At this step, we check if the inverter and the transformer are capable of driving the multiplier at the desired condition, and if not, revise their designs. In our design, within the frequency range that is feasible for the inverter and the transformer, 1 MHz is found to achieve the highest voltage gain of the multiplier.

As a final step, capacitance is added to the class-E inverter if necessary in order to modify the resonant capacitance for soft switching of Q_1 at this frequency. In our design, the particular set of components we chose allowed Q_1 to achieve soft switching without any additional capacitance (and therefore additional mass). We experimentally confirm that the multiplier is driven with the frequency and amplitude found in the previous step when connected to the rest of the

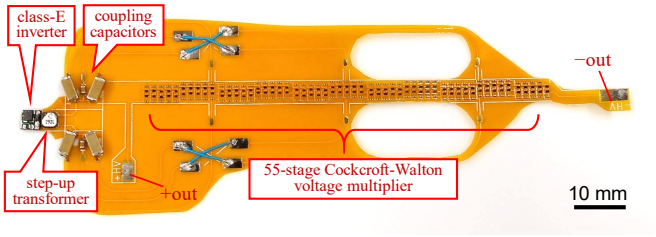

(a)

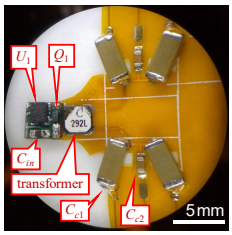

(b)

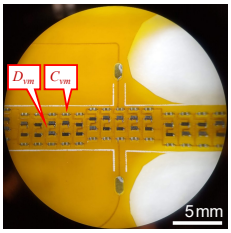

(c)

Fig. 7. Photograph of the implemented high voltage power supply. Scale bar is located in bottom right corner of each picture. (a) Overall view. (b) Close-up view of the inverter, transformer, and coupling capacitors. (c) Close-up view of the voltage multiplier.

TABLE III
MASS BREAKDOWN OF THE POWER SUPPLY. PART NAMES ARE IN REFERENCE TO FIG. 6.

Name	Parts count	Mass per part [mg]	Occupied PCB mass per part [mg]	Total accountable mass [mg]
U_1	1	2	2	4
C_{in}	1	1	1	2
Q_1	1	1	1	2
transformer	1	52	3	55
C_{c1}	4	118	4	488
C_{c2}	2	5	1	12
C_{vm}	109	0.4	0.2	65
D_{vm}	110	0.2	0.2	44
FR4 board for inverter†	–	–	–	25
unoccupied flex PCB*†	–	–	–	181
etc.**†	–	–	–	73
sum				951

*Most of the unoccupied PCB area was used for interconnection between coupling capacitors and the voltage multiplier.
**Mostly solder and jump wires.
†Used for convenience of testing; can be removed or reduced substantially in optimized design.

power supply, and complete the design.

Fig. 7 shows the implemented power supply as a result of the design process. Table III provides the mass breakdown of the circuit. The complete circuit is assembled on a 0.08 mm thick polyimide flexible PCB. The circuit masses 951 mg, which can be reduced by the removal of non-essential items marked with a dagger symbol (†) in the table. With 3.7 V supply voltage, 333 mW input power, and 100 MΩ load resistor, the output dc voltage of 4.321 kV is measured. The resulting figure of merit following the definition from (1) is 19.6 kV^2/g. The final schematic and part list are given in Fig. 6 and Table II.

TABLE IV
EXPERIMENTAL CONDITIONS FOR THE DEMONSTRATION OF A PERCHING MAV.

Electroadhesive pad	**mass**: 2 g **size**: 10 cm ×10 cm **leakage**: < 1 µA at 6 kV **material**: polyimide flexible PCB
MAV	**mass**: 17 g **battery**: 3.7 V, 150 mAh **measured flight time**: 7 min 2 sec **model number**: Eachine E10C
Perching MAV (pad, circuit, & MAV)	**mass**: 20.4 g **height**: 15 cm **measured flight time**: 6 min 24 sec

IV. UNTETHERED PERCHING OF A MAV

For a demonstration of design efficacy, a commercial drone (Eachine E10C) with an electroadhesion pad and the high voltage power supply attached is shown to fly up (manually piloted) and perch on a ceiling without requiring any external supply tethers. As the pre-existing firmware flight controllers were used without modification, the adhesion pad is placed several rotor diameters away and on-axis with the initial center of mass in order to minimize any introduced instability.

Table IV describes the experimental conditions. Fig. 1 shows the perching-capable MAV system consisting of the quadrotor, the power supply, the electroadhesive pad, and a balsa wood stick providing structural support. The high voltage power supply was powered directly by the on-board battery. This experiment was performed without the capacity to un-perch (i.e., with the converter always powered and biasing the electroadhesive pad) due to the inability to directly modify the quadrotor control circuitry or firmware. Pad detachment could theoretically be realized without additional circuit components through a wirelessly-switchable connection between the onboard flight controller and the converter oscillator "Standby" pin, although the residual surface charge that holds the pad may take up to hours to disappear completely [12]. For faster un-perching, polarity reversal [27] or mechanical means [28]–[30] could be employed at the cost of extra payload mass.

Fig. 8 shows the electroadhesive pad and its adhesive force at various voltages. The force initially increases proportionally to the voltage squared as described in [12], [15], [16], then saturates at the 5 to 6 kV range, which is similar to the behavior observed in [31]. The pad generates an electrostatic force close to 300 gram-force with 4.32 kV applied voltage from the power supply. This force was deemed enough to attach the MAV on the ceiling even with the potentially non-ideal surface conditions present during the real test.

Fig. 9 shows combined snapshots of the perching MAV during its operation. Since the electroadhesive pad as shown does not attach well to the rough surface of this particular ceiling, we covered a small section of the ceiling with glossy magazine pages that we used for measurements in Fig. 8b. Then, we hard-wired the high voltage power supply to the on-board battery and flew the drone upwards until the pad made contact with the ceiling. Finally, we turned off all the

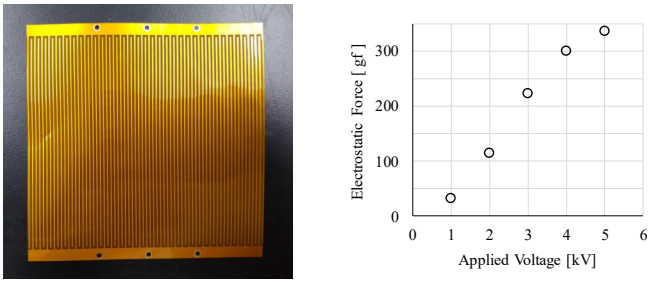

(a) (b)

Fig. 8. The implemented electroadhesive pad. (a) Photo of the 10 cm × 10 cm pad, made of a polyamide-based flexible PCB. The width of each electrode 'fingers' and the spacing between them are 0.76 mm (30 mils). (b) A plot of the measured electrostatic pressure versus applied voltage. Following the protocol used in [10], the force was measured using a force gauge pulled perpendicularly after 60 seconds of attachment, followed by 6 minutes of dielectric relaxation time.

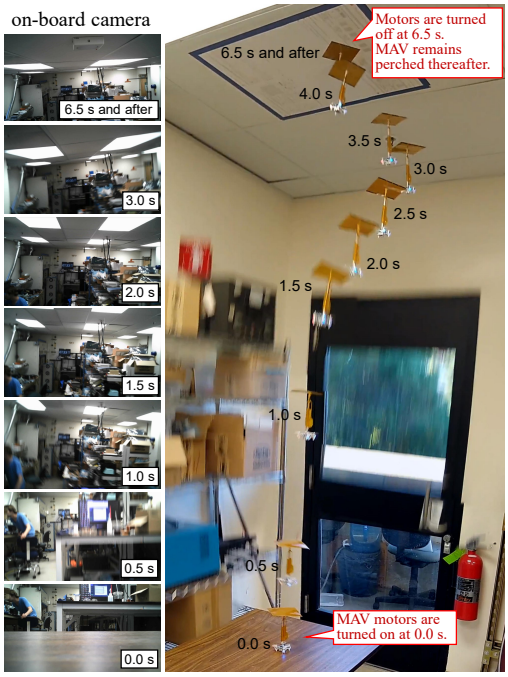

Fig. 9. Demonstration of electroadhesive perching of the MAV. The vehicle flies upward from 0.0 s to 6.5 s, attaches to the ceiling at 6.5 s, and remains perched after 6.5 s timestamp. The figure displays the flight of the vehicle (right) with the recording from the vehicle's on-board camera (left).

motors of the quadrotor and observed that the MAV remained attached on the ceiling. The supplementary video shows the flight of the MAV with the recording from the drone's on-board camera.

The duration for which the vehicle can remain perched on the ceiling is about 100 minutes, which is almost 15 times longer than the vehicle's flight time. This duration is estimated from the high voltage generator's measured power consumption of 333 mW and the battery's energy capacity of 3.7 V, 150 mAh. The single-charge flight time of the vehicle is 7 minutes and 2 seconds before the perching mechanism is mounted on board, and 6 minutes and 24 seconds after it is installed. In contrast, if the extra 3.4 g of payload (pad, power supply, and structural support) was used for additional energy storage instead of perching, the flight time would only increase by about 5 minutes and 20 seconds (using 125 Wh/kg for the specific energy of the lithium-polymer battery) to ≈ 12 minutes.

As a final note, the electroadhesive pad in Fig. 8 is a non-optimal design in terms of adhesion performance, meant only for demonstration of the power supply's capability. Such sub-optimality was deemed excusable because the power supply design is mostly independent from the specifics of the electroadhesive pad design. The adhesive pressure generated by this pad is only half of the "worst-case" pressure given by [10] at 1 kV potential, and almost 7 times less than the worst case from [18] at 4 kV potential. Although a more optimal pad design would require a lower output voltage for perching of this particular MAV and therefore require a lower mass high voltage supply, this does not directly translate to a change in the proposed specific voltage figure of merit.

V. Conclusion

In this paper, we have presented a high voltage power supply that, from a lithium polymer battery input, is both light enough to be mounted on many micro air vehicles and capable of generating the high voltage required for successful electroadhesive perching. We have proposed a figure of merit – the specific voltage – that captures the application-specific performance of the power supply, and showed that the presented power supply outperforms existing designs for the purpose of electroadhesive perching. To show the usefulness of this approach, we attached the power supply and an un-optimized electroadhesive pad to a small commercial quadrotor and demonstrated for the first time a vehicle that can fly and perch using this mechanism independently, with no tether attached.

Beyond being useful for enabling electroadhesive perching of quadrotors, the proposed figure of merit in this work is also valuable for the design and analysis of power supplies intended for robotic actuators at similar high voltage, low power design points (e.g., dielectric elastomer [32], piezoelectric [33], electrostatic [34], [35], electroadhesive [36]–[38] and electrohydrodynamic [39]). The higher FOM of the converter described here implies that, given adjustment of component values to meet the specific output requirements of the platform, it would potentially be a superior solution in terms of payload mass to prior efforts in this space.

Appendix

Table V and VI list MAVs, UAVs, and power supplies in our survey for generating plots in Fig. 3 and 4. (*Table VI has been omitted to meet the IROS page limit. To see the full list, check the RA-L version of this paper*: `ieeexplore.ieee.org/abstract/document/9113652/`)

References

[1] R. C. Michelson, "Overview of micro air vehicle system design and integration issues," *Ency. Aerospace Eng.*, 2010.

[2] W. R. Davis, B. B. Kosicki, D. M. Boroson, and D. Kostishack, "Micro air vehicles for optical surveillance," *Lincoln Lab. J.*, vol. 9, no. 2, pp. 197–214, 1996.

TABLE V
LIST OF MAVS AND UAVS IN OUR SURVEY.

Name	Length [cm] (l_{mav})	Mass [g] (m_{mav})
DelFly Micro	10	3.07
10 cm Ornithopter	10	4.72
PD-100 Black Hornet Nano	12	16
QR W100	12	76
Mini X6	13	52
Seiko-Epson uFR-II	13.6	12.3
QR W100S	14.4	89
15 cm Ornithopter	15	8.7
Black Widow	15	56.5
Nano Hummingbird	16.5	19
MicroBat	22.9	12.5
QR Y100	25.2	146
H2Bird	26.5	13.2
DelFly Explorer	28	20
28 cm Ornithopter	28	30.6
Parrot Bebop 2	29	525
H301S	32	164
Bionic Bird	33	9.07
Avitron V2.0	33	8.5
36 cm Ornithopter	36	44.6
DJI Phantom 2	37.1	1000
AR Drone 2.0	58.4	380
350 QX2	59.4	3403
eBee	96	690
Wasp AE RQ-12A	102	1300

[3] D. J. Pines and F. Bohorquez, "Challenges facing future micro-air-vehicle development," *J. aircraft*, vol. 43, no. 2, pp. 290–305, 2006.

[4] T. Hylton, C. Martin, R. Tun, and V. Castelli, "The darpa nano air vehicle program," in *50th AIAA Aerospace Sci. Meeting including the New Horizons Forum and Aerospace Expo.*, 2012, p. 583.

[5] Y. Mulgaonkar, M. Whitzer, B. Morgan, C. M. Kroninger, A. M. Harrington, and V. Kumar, "Power and weight considerations in small, agile quadrotors," in *Micro-and Nanotech. Sensors, Sys., and App. VI*, vol. 9083. Int'l Society for Optics and Photonics, 2014, p. 90831Q.

[6] B. Araki, J. Strang, S. Pohorecky, C. Qiu, T. Naegeli, and D. Rus, "Multi-robot path planning for a swarm of robots that can both fly and drive," in *Int'l Conf. Robot. Auto. (ICRA)*. IEEE, 2017, pp. 5575–5582.

[7] M. Kovač, J. Germann, C. Hürzeler, R. Y. Siegwart, and D. Floreano, "A perching mechanism for micro aerial vehicles," *J. Micro-Nano Mechatronics*, vol. 5, no. 3-4, pp. 77–91, 2009.

[8] D. Floreano and R. J. Wood, "Science, technology and the future of small autonomous drones," *Nature*, vol. 521, no. 7553, pp. 460–466, 2015.

[9] J. Thomas, J. Polin, K. Sreenath, and V. Kumar, "Avian-inspired grasping for quadrotor micro uavs," in *Int'l Design Eng. Tech. Conf. and Computers and Info. in Eng. Conf.* American Society of Mechanical Engineers Digital Collection, 2013.

[10] M. Graule, P. Chirarattananon, S. Fuller, N. Jafferis, K. Ma, M. Spenko, R. Kornbluh, and R. Wood, "Perching and takeoff of a robotic insect on overhangs using switchable electrostatic adhesion," *Science*, vol. 352, no. 6288, pp. 978–982, 2016.

[11] R. J. Wood, B. Finio, M. Karpelson, K. Ma, N. O. Pérez-Arancibia, P. S. Sreetharan, H. Tanaka, and J. P. Whitney, "Progress on 'pico'air vehicles," *Int'l J. Robot. Research*, vol. 31, no. 11, pp. 1292–1302, 2012.

[12] G. J. Monkman, "An analysis of astrictive prehension," *The Int'l J. Robot. Research*, vol. 16, no. 1, pp. 1–10, 1997.

[13] J. P. D. Téllez, J. Krahn, and C. Menon, "Characterization of electro-adhesives for robotic applications," in *Int'l Conf. Robot. Biomimetics*, Dec 2011, pp. 1867–1872.

[14] S. Park, A. Goldin, and J. Rivas-Davila, "Miniature high-voltage dc-dc power converters for space and micro-robotic applications," in *Energy Conv. Congress and Expo. (ECCE)*, Sep. 2019, pp. 2007–2014.

[15] K. H. Koh, R. K. Chetty, and S. Ponnambalam, "Modeling and simulation of electrostatic adhesion for wall climbing robot," in *Int'l Conf. Robot. Biomimetics*. IEEE, 2011, pp. 2031–2036.

[16] J. Guo, T. Bamber, M. Chamberlain, L. Justham, and M. Jackson, "Optimization and experimental verification of coplanar interdigital electroadhesives," *J. Phys. D: App. Phys.*, vol. 49, no. 41, p. 415304, 2016.

[17] L. Petricca, P. Ohlckers, and C. Grinde, "Micro-and nano-air vehicles: State of the art," *Int'l J. Aerospace Eng.*, vol. 2011, 2011.

[18] H. Prahlad, R. Pelrine, S. Stanford, J. Marlow, and R. Kornbluh, "Electroadhesive robots–wall climbing robots enabled by a novel, robust, and electrically controllable adhesion technology," in *Int'l Conf. Robot. Aut.* IEEE, 2008, pp. 3028–3033.

[19] O. Unver and M. Sitti, "A miniature ceiling walking robot with flat tacky elastomeric footpads," in *2009 IEEE Int'l Conf. Robot. Auto.* IEEE, 2009, pp. 2276–2281.

[20] D. Schmidt, C. Hillenbrand, and K. Berns, "Omnidirectional locomotion and traction control of the wheel-driven, wall-climbing robot, cromsci," *Robotica*, vol. 29, no. 7, pp. 991–1003, 2011.

[21] N. Bertoni, G. Frattini, R. G. Massolini, F. Pareschi, R. Rovatti, and G. Setti, "An analytical approach for the design of class-e resonant dc–dc converters," *IEEE Trans. Power Electron.*, vol. 31, no. 11, pp. 7701–7713, 2016.

[22] S. Park and J. Rivas-Davila, "Duty cycle and frequency modulations in class-e dc–dc converters for a wide range of input and output voltages," *IEEE Trans. Power Electron.*, vol. 33, no. 12, pp. 10 524–10 538, 2018.

[23] Z. Zhang, K. Xu, Z.-W. Xu, J. Xu, X. Ren, and Q. Chen, "Gan vhf converters with integrated air-core transformers," *IEEE Trans. Power Electron.*, vol. 34, no. 4, pp. 3504–3515, 2018.

[24] J. Kuffel and P. Kuffel, *High voltage engineering fundamentals*. Elsevier, 2000.

[25] M. S. Naidu and V. Kamaraju, *High Voltage Engineering*. McGraw-Hill, 2010.

[26] S. Ray, *Introduction To High Voltage Engineering*. PHI Learning, 2013.

[27] H. E. Prahlad, R. E. Pelrine, P. A. Von Guggenberg, R. D. Kornbluh, and J. S. Eckerle, "High voltage converters for electrostatic applications," Jul. 25 2013, uS Patent App. 13/356,300.

[28] G. Monkman, P. Taylor, and G. Farnworth, "Principles of electroadhesion in clothing robotics," *Int'l J. Clothing Sci. Tech.*, vol. 1, no. 3, pp. 14–20, 1989.

[29] G. Monkman, "Electroadhesive microgrippers," *Industrial Robot: An Int'l J.*, 2003.

[30] X. Gao, C. Cao, J. Guo, and A. Conn, "Elastic electroadhesion with rapid release by integrated resonant vibration," *Adv. Materials Tech.*, vol. 4, no. 1, p. 1800378, 2019.

[31] K. H. Koh, M. Sreekumar, and S. Ponnambalam, "Experimental investigation of the effect of the driving voltage of an electroadhesion actuator," *Materials*, vol. 7, no. 7, pp. 4963–4981, 2014.

[32] Y. Chen, H. Zhao, J. Mao, P. Chirarattananon, E. F. Helbling, N.-s. P. Hyun, D. R. Clarke, and R. J. Wood, "Controlled flight of a microrobot powered by soft artificial muscles," *Nature*, vol. 575, no. 7782, pp. 324–329, 2019.

[33] N. T. Jafferis, E. F. Helbling, M. Karpelson, and R. J. Wood, "Untethered flight of an insect-sized flapping-wing microscale aerial vehicle," *Nature*, vol. 570, no. 7762, pp. 491–495, 2019.

[34] D. S. Contreras, D. S. Drew, and K. S. Pister, "First steps of a millimeter-scale walking silicon robot," in *Int'l Conf. Solid-State Sensors, Actuators and Microsys. (TRANSDUCERS)*. IEEE, 2017, pp. 910–913.

[35] Z. Liu, X. Yan, M. Qi, and L. Lin, "Electrostatic flapping wings with pivot-spar brackets for high lift force," in *Int'l Conf. Micro Electro Mech. Sys. (MEMS)*. IEEE, 2016, pp. 1133–1136.

[36] M. Taghavi, T. Helps, and J. Rossiter, "Electro-ribbon actuators and electro-origami robots," *Sci. Robotics*, vol. 3, no. 25, p. eaau9795, 2018.

[37] G. Gu, J. Zou, R. Zhao, X. Zhao, and X. Zhu, "Soft wall-climbing robots," *Sci. Robotics*, vol. 3, no. 25, p. eaat2874, 2018.

[38] S. D. de Rivaz, B. Goldberg, N. Doshi, K. Jayaram, J. Zhou, and R. J. Wood, "Inverted and vertical climbing of a quadrupedal microrobot using electroadhesion," *Sci. Robotics*, vol. 3, no. 25, p. eaau3038, 2018.

[39] D. S. Drew, N. O. Lambert, C. B. Schindler, and K. S. Pister, "Toward controlled flight of the ionocraft: a flying microrobot using electrohydrodynamic thrust with onboard sensing and no moving parts," *IEEE Robot. Autom. Lett.*, vol. 3, no. 4, pp. 2807–2813, 2018.